THE UNIVERSITY *of* EDINBURGH

Edinburgh Research Explorer

Nonmagnetic spin-singlet dimer formation and coupling to the lattice in the 6H perovskite Ba3CaRu2O9

OPEN ACCESS

Nonmagnetic spin-singlet dimer formation and coupling to the lattice in the 6H perovskite Ba$_3$CaRu$_2$O$_9$**

Mark S Senn,[1,3] Angel M Arevalo-Lopez,[1] Takashi Saito,[2] Yuichi Shimakawa[2] and J Paul Attfield[1]

[1]EaStCHEM, Centre for Science at Extreme Conditions, Joseph Black Building, University of Edinburgh, West Mains Road, Edinburgh, EH9 3JJ, UK.

[2]Institute for Chemical Research, Kyoto University, Uji, Kyoto 611-0011, Japan.

[3]Present address: Diamond Light Source Ltd, Harwell Science and Innovation Campus, Didcot OX11 0DE, UK.

[*]Corresponding author; e-mail: j.p.attfield@ed.ac.uk

Supporting information:
Online supplementary data available from http://www.stacks.iop.org/JPhysCM/25/496008/mmedia

Abstract

Non-conservation of magnetic neutron scattering from the six-layer hexagonal perovskite $Ba_3CaRu_2O_9$ on cooling reveals that $(Ru^{5+})_2$ dimers form nonmagnetic spin-singlet ground states. This is in contrast to $Ba_3BRu_2O_9$ (B=Co or Ni) analogues which display long range spin ordered ground states containing antiferromagnetic $(Ru^{5+})_2$ dimers (Lightfoot and Battle 1990 *J. Solid State Chem.* **89** 174). Dimer formation is weakly coupled to the lattice, resulting in an excess [101] microstrain broadening of diffraction peaks at low temperatures. Non-conservation of magnetic neutron scattering is also observed around the charge ordering transition in $Ba_3NaRu_2O_9$ showing that the ground state structure is coupled to spin-singlet formation in charge ordered Ru_2O_9 dimers.

1. Introduction

Coupling of spin or orbitally ordered states into small clusters in transition metal compounds gives rise to many physical phenomena. The formation of orbital molecules—weakly bonded clusters of transition metals within an orbitally ordered insulator—has recently been recognized in several systems, for example in the spinels AlV_2O_4 containing heptameric $S = 0$ spin orbital molecules [1], and magnetite, Fe_3O_4, where $S = 1/2$ trimerons have been reported [2, 3]. In addition, electronic structure calculations on $Ba_4Ru_3O_{10}$ have proposed the formation of Ru trimers to account for the observation of reduced magnetic moments and unconventional antiferromagnetism [4]. The simplest case of spin clustering is the formation of nonmagnetic singlet dimers in $S = 1/2$ systems which can display Bose–Einstein magnon condensation, e.g. in $TlCuCl_3$ [5], and spin-liquid ground states, e.g. in DQVOF [6]. Here we demonstrate that $S = 3/2$ Ru^{5+} ions in 6H perovskites which contain a triangular lattice of Ru_2O_9 dimers form nonmagnetic spin-singlet dimers in the absence of an additional magnetic cation, and a weak lattice signature accompanying dimer formation in $Ba_3CaRu_2O_9$ is discovered.

Many six-layer hexagonal (6H) perovskites of the type $Ba_3BRu_2O_9$ are known and the formal Ru charge may be varied from 4+ to 5.5+ by substitution of various B cations [7–9]. Most derivatives crystallize in the aristotype 6H structure (space group $P6_3/mmc$) shown in figure 1, but those with B = Sr [10] and Cu [11] have lower, monoclinic, symmetry at ambient conditions. Low temperature lattice distortions may be driven by charge or spin orders. Charge order of $(Ru^{5+})_2O_9$ and $(Ru^{6+})_2O_9$ dimers, accompanied by the opening of a spin gap and a structural distortion to monoclinic $P2/c$ symmetry, was recently observed at 210 K in $Ba_3NaRu_2O_9$ [12]. The opening of a spin gap has also been reported in $Ba_3BiRu_2O_9$, coupled with a transition to $C2/c$ symmetry at 176 K [13]. Long range magnetic order in $Ba_3B^{2+}(Ru^{5+})_2O_9$ 6H perovskites has only been observed by neutron diffraction for B=Co^{2+} and Ni^{2+} where antiferromagnetic $(Ru^{5+})_2O_9$ spin dimers are antiferromagnetically coupled to the Co^{2+} or Ni^{2+} spins [11, 14, 15]. Long range antiferromagnetic order in $Ba_3CoRu_2O_9$ drives a hexagonal to orthorhombic structural transition at 93 K [15].

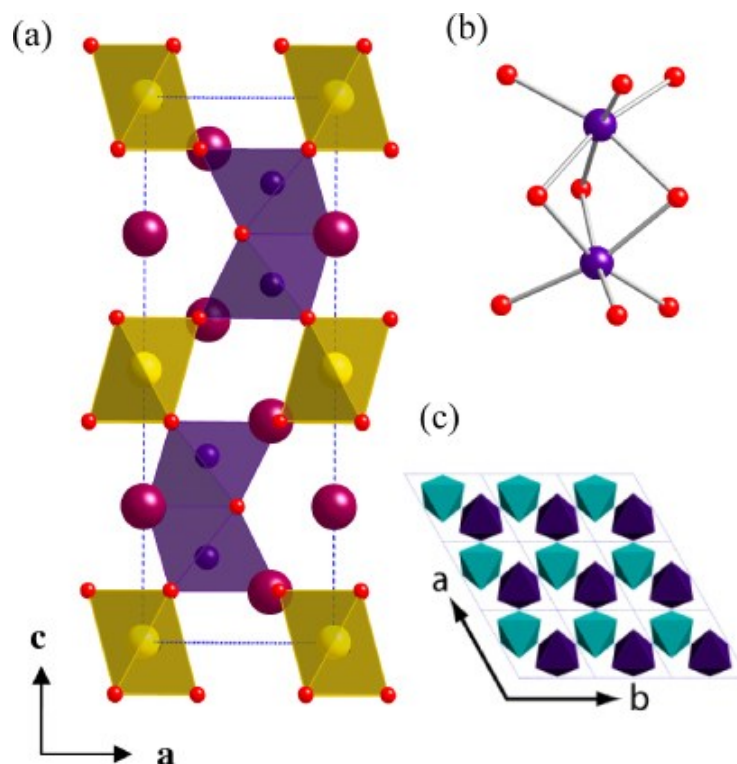**Figure 1.** Crystal structure of $Ba_3CaRu_2O_9$: (a) stacking sequence in the *ac* plane with Ba/Ca/Ru/O atoms shown as large (dark red)/medium (yellow)/small (purple)/very small (scarlet) spheres; (b) a Ru_2O_9 dimer, (c) the arrangement of the Ru_2O_9 dimers on the triangular lattice in the *ab* plane at $z = 1/4$ (light blue) and $z = 3/4$ (dark purple).

A reported suppression of magnetic susceptibility towards zero at ~50 K in $Ba_3CaRu_2O_9$ was fitted using a model of interacting antiferromagnetic dimers [8]. However, the 4.2 K ^{99}Ru Mössbauer spectrum showed no hyperfine splitting, suggesting that magnetism may be suppressed through spin-singlet formation [16]. No long range magnetic order was observed at 4 K in an initial neutron diffraction study, and inelastic neutron scattering evidenced a ~25 meV magnon that was assigned to the $S = 0 \rightarrow S = 1$ dimer excitation [17]. We have reinvestigated $Ba_3CaRu_2O_9$ using susceptibility measurements and x-ray and neutron diffraction to probe the magnetic ground state and investigate low temperature structural instabilities. We also report further insights into the ground state of $Ba_3NaRu_2O_9$.

2. Experimental details

A 10 g sample of $Ba_3CaRu_2O_9$ was prepared by calcining a pellet made from stoichiometric amounts of RuO_2, $BaCO_3$ and $CaCO_3$ at 900 ° C. The pellet was then heated to 1000 ° C for 48 h with multiple cycles of regrinding and repelletization. The polycrystalline sample was found to be phase pure by laboratory x-ray

diffraction. High resolution synchrotron x-ray powder diffraction data ($\lambda = 0.50\,014(2)$ Å) at beamline BL19B2, SPring-8, were collected in the temperature range 120–300 K. High resolution neutron powder diffraction data were collected at WISH [18], ISIS, to a *d*-spacing limit of 45 Å (minimum scattering vector $Q = 0.14$ Å^{-1}) at 1.6, 80 and 150 K. All profile fits were performed using the TOPAS-Academic program [19]. Zero field cooled susceptibility data were measured in the range 2–400 K in a 5 kOe applied field.

3. Results and discussion

3.1. Ba$_3$CaRu$_2$O$_9$ spin dimerization

The absence of magnetic diffraction peaks at 1.6 K (figure 2(a)) confirms that no long range spin order is present in Ba$_3$CaRu$_2$O$_9$. Local interactions between neighbouring t_{2g}^3 $S = 3/2$ Ru^{5+} ions could result in the formation of antiferromagnetic or of nonmagnetic spin-singlet dimers, both with net spin $S = 0$. These two possibilities can be distinguished according to whether they conserve magnetic neutron scattering. Local antiferromagnetic order of Ru^{5+} $S = 3/2$ spins into dimers at low temperatures will conserve the total magnetic scattering with respect to the high temperature paramagnetic state, but the formation of nonmagnetic dimers leads to a net loss of magnetic neutron scattering on cooling. The WISH diffractometer measures scattered neutrons over a wide time-of-flight range, equivalent to $Q = 0.14$–35 Å^{-1} for elastic scattering, and with inelastically scattered neutrons recorded as part of the background. Hence changes in the WISH spectrum with temperature may be used as an approximate measure of changes of the magnetic scattering cross section.

To validate this approach the difference spectrum for a related 6H material, Ba$_3$LaRu$_2$O$_9$, is shown in figure 2(b). This has a conventional antiferromagnetic ordering below a temperature of $T_N = 22$ K [20, 21] so magnetic scattering should be conserved through the transition. The difference between WISH spectra collected at temperatures above (40 K) and below (1.6 K) T_N shows positive intensity from 40 K paramagnetic scattering, and negative peaks from antiferromagnetic order at 1.6 K. The averaged intensity difference across the data range of 0.004 ± 0.004 units is not statistically significant and validates the use of the WISH difference function as an approximate measure of conservation of magnetic neutron scattering.

The difference between WISH neutron scattering spectra for Ba$_3$CaRu$_2$O$_9$ at 80 and 1.6 K in figure 2(a) differs significantly from that of Ba$_3$LaRu$_2$O$_9$ due to the absence of low temperature ordering features. The function is positive at virtually all points and the average intensity difference between $Q = 0.15$ and 35 Å^{-1} is 0.013 ± 0.002 units. Hence a significant loss of magnetic scattering is observed for Ba$_3$CaRu$_2$O$_9$, demonstrating that paramagnetic Ru^{5+} $S = 3/2$ spins condense into nonmagnetic $S = 0$ dimers on cooling from 80 to 1.6 K, in keeping with a previous ^{99}Ru Mössbauer observation [16].
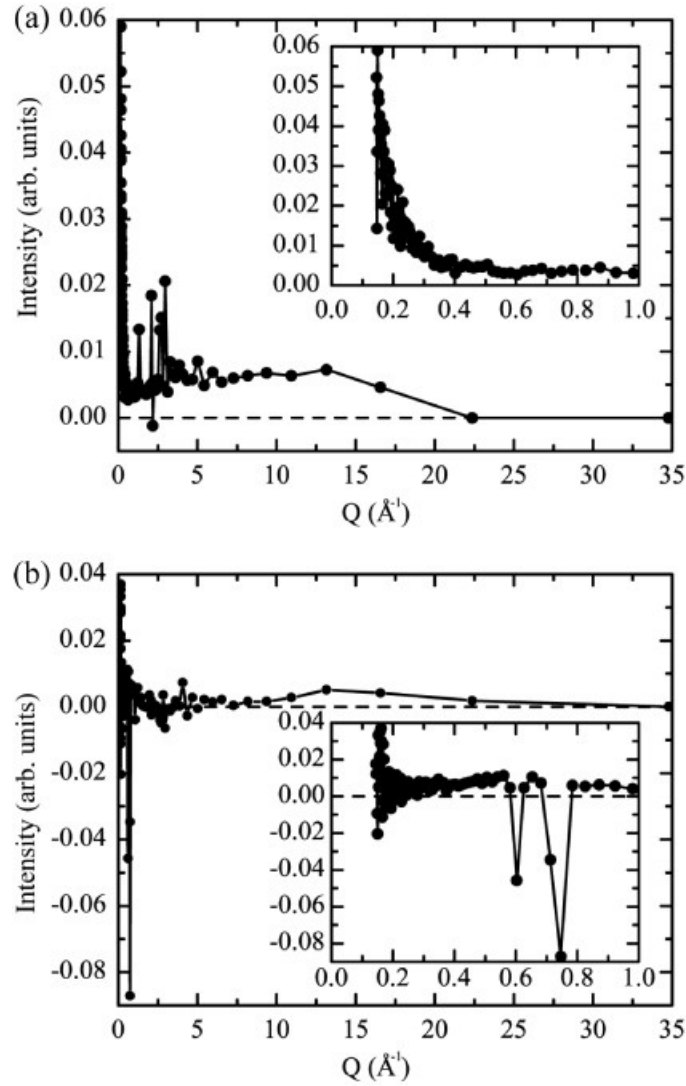
Figure 2. (a) Difference in neutron scattering intensity from $Ba_3CaRu_2O_9$ obtained by subtracting 1.6 K data from an 80 K spectrum. (b) Difference in neutron scattering intensity from $Ba_3LaRu_2O_9$ obtained by subtracting 1.6 K data from a 40 K spectrum. Expansions of low-Q data where magnetic peaks may appear as negative features are in the inset. The main plots are constructed from the forward- ($Q = 0.15$–2 $Å^{-1}$) and back-scattering ($Q = 2$–35 $Å^{-1}$) banks of WISH.

The magnetic susceptibility of $Ba_3CaRu_2O_9$ in figure 3 decreases smoothly on cooling below 400 K as reported previously [8], with a small upturn below 50 K due to a trace of paramagnetic impurity. The susceptibility per mole of Ru spins χ has been fitted using a standard expression for a dimer of $S = 3/2$ ions [22] plus Curie impurity (A/T) and temperature-independent (B) terms:

$$\chi = (Ng^2\mu_B^2/k_BT)\{[\exp(2J/k_BT) + 5\exp(6J/k_BT) \\ + 14\exp(12J/k_BT)]/[1 + 3\exp(2J/k_BT) \\ + 5\exp(6J/k_BT) + 7\exp(2J/k_BT)]\} + (A/T) + B$$

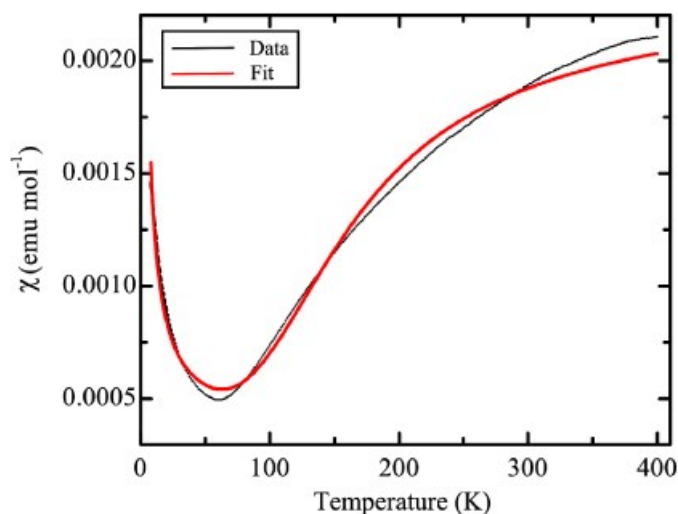giving an intradimer coupling energy of $J/k_B = -240(1)$ K.

Figure 3. Fit of the function described in the text (red line) to magnetic susceptibility data (black line) for $Ba_3CaRu_2O_9$.

3.2. $Ba_3CaRu_2O_9$ lattice strain

Rietveld fitting of low temperature powder x-ray and neutron diffraction data did not reveal any structural phase transitions in $Ba_3CaRu_2O_9$. However, an increased broadening of diffraction peaks was observed on cooling, as shown in figure 4 for the 120 K synchrotron x-ray pattern. Isotropic microstrain models (see figure 4(a)) do not account for this as selective peak broadening is evident. Lattice distortions from hexagonal $P6_3/mmc$ to monoclinic $C2/c$ symmetry are observed in some 6H perovskites, and inclusion of a monoclinic lattice distortion improves the fit but does not account for all broadenings (figure 4(b)). A good fit to the synchrotron data (figure 4(c)) and to the WISH neutron data (figure 5) was obtained using the method of Stephens, where anisotropic broadening of the hexagonal diffraction peaks was modelled by refining three independent microstrain covariance parameters S_{400}, S_{202} and S_{004} [23]. Refinement results are shown as supplemental material[4]. The lattice parameters in figure 6(a) show conventional thermal behaviour with similar expansions of the *a* and *c* parameters.
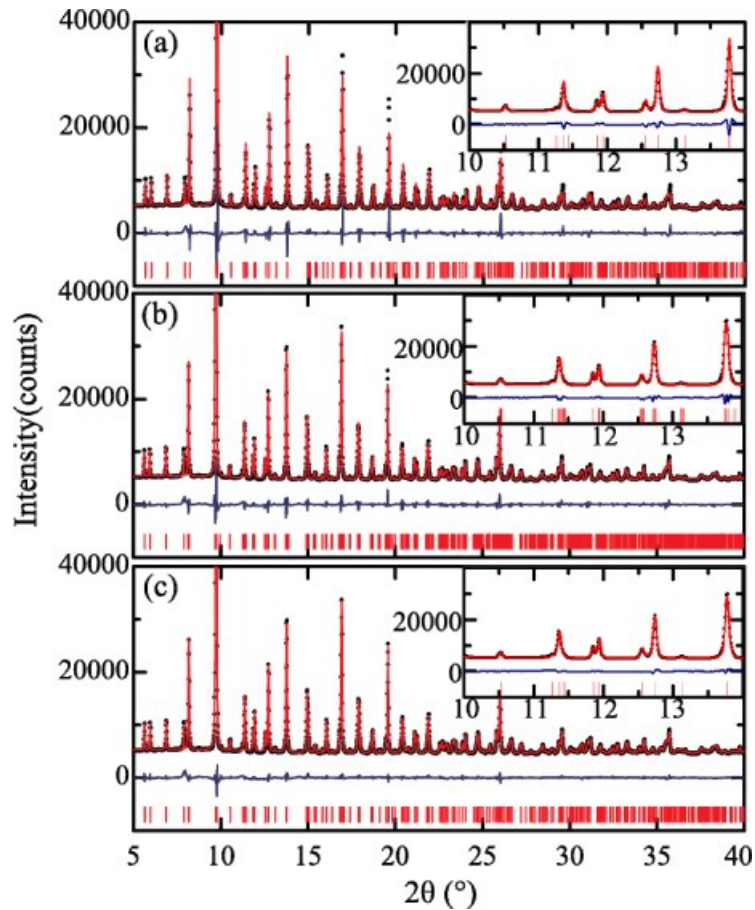
Figure 4. Rietveld refinement fits to 120 K synchrotron data for $Ba_3CaRu_2O_9$ with (a) an isotropic peak broadening model (fitting residuals $\chi^2 = 3.31$, $R_{wp} = 4.37\%$), (b) isotropic peak broadening and a refined monoclinic distortion ($\chi^2 = 2.24$, $R_{wp} = 2.95\%$), and (c) a three parameter Stephens anisotropic peak broadening model ($\chi^2 = 1.60$, $R_{wp} = 2.11\%$). Insets show the fits in the $2\theta = 10°–14°$ regions.

Figure 5. Rietveld refinement against neutron data collected from the back-scattering bank of WISH for $Ba_3CaRu_2O_9$ at 1.6 K. The inset shows the fit in the $d = 1.4–2.0$ Å region.

Figure 6. Evolution of (a) lattice parameters and (b) microstrains with temperature for $Ba_3CaRu_2O_9$ from Rietveld refinement against powder x-ray (open symbols) and neutron (cl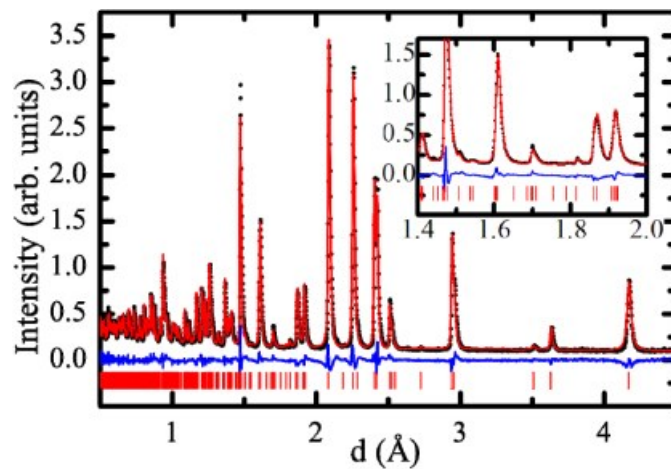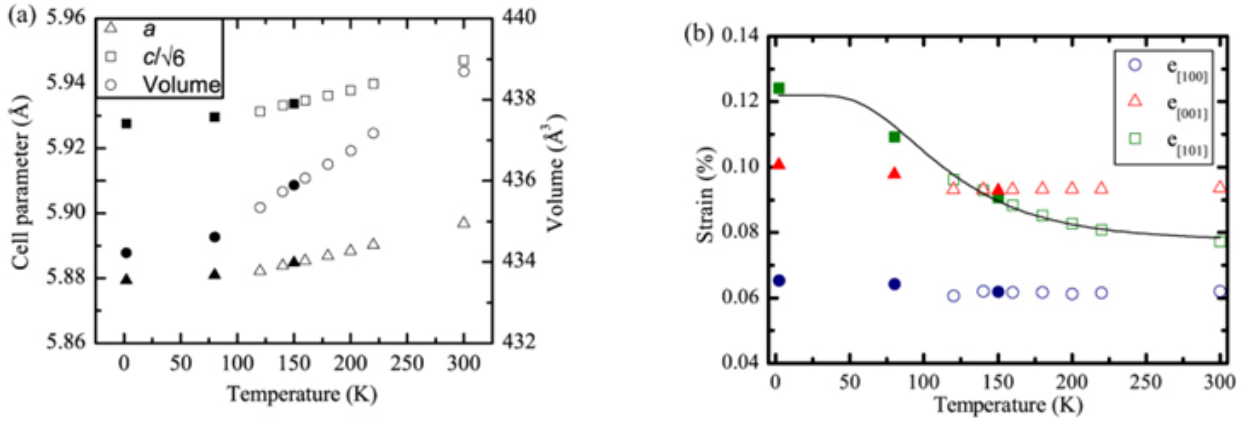osed symbols) data. Neutron lattice parameters have been scaled against x-ray values. Error bars are smaller than the points. The fit of the function described in the text to the $\Delta e_{[101]}$ excess microstrain after subtraction of a 0.073% constant term is shown in (b).

Strain variances e in the [100], [001] and [101] hexagonal lattice directions were derived from the refined covariance parameters S and are shown in figure 6(b). The $e_{[100]}$ and $e_{[001]}$ microstrains are almost constant over the temperature range 1.6–300 K, and the higher value for $e_{[001]}$ may reflect some stacking faults or polytype intergrowths in the c-direction. However, $e_{[101]}$ shows a strong temperature dependence and increases greatly on cooling. This microstrain describes local deviations in the α or β angles of the hexagonal lattice from 90° and hence the enhancement on cooling is consistent with an incipient distortion to monoclinic symmetry. This is supported by a ^{117}Cd Mossbauer study of $Ba_3CaRu_2O_9$ where Cd was doped for Ca, which reported evidence for quadrapolar splitting at low temperatures consistent with local monoclinic symmetry [24].

The gradual increase in $e_{[101]}$ with cooling towards an apparent maximum at $T = 0$ is not consistent with a conventional structural transition, but suggests that the excess microstrain may be generated by the formation of $(Ru^{5+})_2$ dimers. Coupling to the lattice is likely to be through shortening of the Ru–Ru distance and local changes in Ru–O bonds. The $\Delta e_{[101]}$ increase in microstrain observed on cooling from high temperature ($T \gg |J|/k_B$) towards $T = 0$ thus depends on the number of ground state dimers N_D. A full description of the variation of $\Delta e_{[101]}$ with N_D would require detailed information about the low temperature microstructure, but as a simple approximation we assume $N_D \sim [1 - \exp(J/k_B T)]$ and $\Delta e_{[101]} \sim N_D^n$ with a temperature-independent exponent n. The function $\Delta e_{[101]} \sim [1 - \exp(-T_D/T)]^n$ with a fitted exponent of $n = 4.7(2)$ describes the thermal variation of excess microstrain well, as shown in figure 6(b). This correlation shows that spin-singlet dimer formation is the likely cause of the anisotropic diffraction peak broadening at low temperatures in $Ba_3CaRu_2O_9$.

3.3. Ba$_3$NaRu$_2$O$_9$ spin dimerization

The non-conservation of magnetic neutron scattering on cooling provides a simple method for evidencing nonmagnetic spin dimer formation, as demonstrated in section 3.1 for Ba$_3$CaRu$_2$O$_9$. The same approach has been applied to neutron diffraction data from a recent study of Ba$_3$NaRu$_2$O$_9$ [12]. In this system an abrupt charge ordering within dimers 2Ru$^{5.5+}_2$O$_9$→Ru$^{5+}_2$O$_9$+Ru$^{6+}_2$O$_9$ drives a structural phase transition at 210 K. Susceptibility drops sharply below the transition and continues to fall down to ~40 K—this variation was fitted by a simple spin-gap expression. Figure 7 compares low-Q neutron scattering data from Ba$_3$NaRu$_2$O$_9$ at several temperatures. The difference between spectra recorded above (300 K) and below (110 K) the charge ordering transition at 210 K reveals a substantial loss of paramagnetic scattering which is not compensated by the appearance of magnetic Bragg peaks. There is little further change of neutron scattering on further cooling from 110 to 1.6 K. Hence the neutron data confirm that nonmagnetic spin-singlet dimers are formed below the charge ordering transition in Ba$_3$NaRu$_2$O$_9$. Neutron scattering profiles at other temperatures would be needed to follow the suppression of magnetic scattering in greater detail and hence distinguish thermal dependences of spin dimerization within the Ru$^{5+}_2$O$_9$ and Ru$^{6+}_2$O$_9$ pairs.
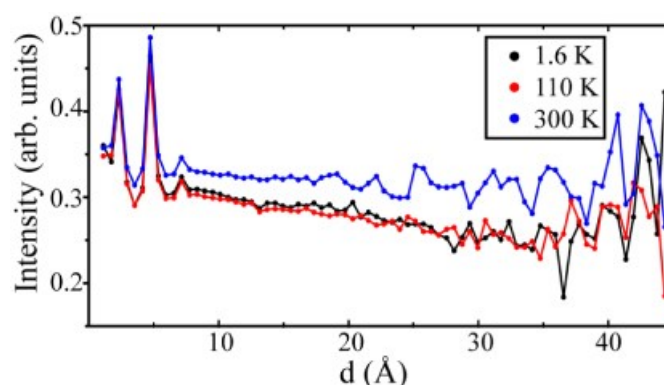

Figure 7. Overlay of powder diffraction data collected on the forward scattering bank of WISH, ISIS, from Ba$_3$NaRu$_2$O$_9$ at several temperatures. The equivalent Q range is 0.14–6.3 Å^{-1}.

4. Conclusions

This study demonstrates that the ground states of (Ru^{5+})$_2$ dimers in 6H Ba$_3$BRu$_2$O$_9$ perovskites can be switched between nonmagnetic and antiferromagnetic spin-singlet states by changing the B^{2+} cation. For nonmagnetic B = Ca, magnetic susceptibility, Mossbauer and neutron scattering data are all consistent with the formation of nonmagnetic dimers. Dimer formation is weakly coupled to the lattice, resulting in an excess [101] microstrain broadening of diffraction peaks. Magnetic B = Co or Ni cations drive the (Ru^{5+})$_2$ dimers into an antiferromagnetic ground state from which long range magnetic neutron diffraction intensities are

observed. Non-conservation of magnetic neutron scattering is also observed around the charge ordering transition in $Ba_3NaRu_2O_9$ showing that the ground state structure contains nonmagnetic Ru_2O_9 dimers, consistent with the presence of nonmagnetic Na^+. The tendency of Ru^{5+} cations to form nonmagnetic spin-singlet dimers in the absence of other magnetic cations may enable quantum magnetic phases to be observed in geometrically frustrated lattices with short Ru–Ru distances.

References

[1] Matsuda K, Furukawa N and Motome Y 2006 *J. Phys. Soc. Japan* **75** 124716.

[2] Senn M S, Wright J P and Attfield J P 2012 *Nature* **481** 173.

[3] Senn M S, Loa I, Wright J P and Attfield J P 2012 *Phys. Rev.* B **85** 125119.

[4] Streltsov S V and Khomskii D I 2012 *Phys. Rev.* B **86** 064429.

[5] Ruegg Ch, Cavadini N, Furrer A, Gudel H-U, Kramer K, Mutka H, Wildes A, Habicht K and Vorderwisch P 2003 *Nature* **423** 62.

[6] Clark L *et al* 2013 *Phys. Rev. Lett.* **110** 207208.

[7] Hinatsu Y and Doi Y 2003 *Bull. Chem. Soc. Japan* **76** 1093.

[8] Darriet J, Drillon M, Villeneuve G and Hagenmuller P 1976 *J. Solid State Chem.* **19** 213.

[9] Stitzer K E, Smith M D, Gemmill W R and zur Loye H C 2002 *J. Am. Chem. Soc.* **124** 13877.

[10] Zandbergen H W and Ijdo D J W 1984 *Acta Crystallogr.* C **40** 919.

[11] Rijssenbeek J T, Huang Q, Erwin R W, Zandbergen H W and Cava R J 1999 *J. Solid State Chem.* **146** 65.

[12] Kimber S A J, Senn M S, Fratini S, Wu H, Hill A H, Manuel P, Attfield J P, Argyriou D N and Henry P F 2012 *Phys. Rev. Lett.* **108** 217205.

[13] Miiller W, Avdeev M, Zhou Q, Studer A J, Kennedy B J, Kearley G J and Ling C D 2011 *Phys. Rev.* B **84** 220406.

[14] Lightfoot P and Battle P D 1990 *J. Solid State Chem.* **89** 174.

[15] Zhou H D, Kiswandhi A, Barlas Y, Brooks J S, Siegrist T, Li G, Balicas L, Cheng J G and Rivadulla F 2012 *Phys. Rev.* B **85** 041201.

[16] Fernandez I, Greatrex R and Greenwood N N 1980 *J. Solid State Chem.* **34** 121.

[17] Darriet J, Soubeyroux J L and Murani A P 1983 *J. Phys. Chem. Solids* **44** 269.

[18] Chapon L C *et al* 2011 *Neutron News* **22** 22.

[19] Senn M S, Kimber S A J, Arevalo-Lopez A M, Hill A H and Attfield J P 2013 *Phys. Rev.* B **87** 134402.

[20] Doi Y, Matsuhira K and Hinatsu Y 2002 *J. Solid State Chem.* **165** 317.

[21] Carlin R L 1986 *Magnetochemistry* (Berlin: Springer) p 94.

[22] Stephens P W 1999 *J. Appl. Crystallogr.* **32** 281.

[23] Yanagida Y, Nakamura J, Asai K, Yamada N, Ohkubo Y, Ambe S, Okada T, Ambe F, Uehara S and
    Kawase Y 1995 *J. Phys. Soc. Japan* **64** 4739